Neuroradiology (2000) 42: 85–91

O. Dietrich
S. Heiland
T. Benner
K. Sartor

Reducing motion artefacts in diffusion-weighted MRI of the brain: efficacy of navigator echo correction and pulse triggering

Received: 31 January 1999
Accepted: 12 July 1999

O. Dietrich (✉) · S. Heiland · T. Benner · K. Sartor
Department of Neuroradiology,
University of Heidelberg Medical School,
Im Neuenheimer Feld 400,
69120 Heidelberg, Germany
e-mail: olaf.dietrich@urz.uni-heidelberg.de,
Tel.: +49-6221-567566,
Fax: +49-6221-564673

Abstract Diffusion-weighted MRI (DWI) is extremely sensitive to motion of the object being examined. Pulse triggering and navigator echo correction are methods for reducing motion artefacts which can be combined with conventional DWI sequences. Implementation of these methods in imaging sequences with a readout of one, three, or five echoes is presented and imaging results compared in a study of five healthy volunteers. As an objective measure for motion-induced image artefacts, the "artefacticity" of an image is defined. Pulse triggering and navigator echo correction significantly improve image quality and provide a technique for high-quality DWI on standard imagers without improved gradient hardware.

Key words Magnetic resonance imaging, diffusion-weighted · Artefacts Navigator echo · Cardiac gating

Introduction

Diffusion-weighted MRI (DWI) of the brain has been shown to be useful for early detection of cerebral ischaemia [1–5] and in monitoring therapy of patients with stroke [6–8]. Other clinical applications include white-matter, fibre-tract imaging by determining diffusion anisotropy [9–12], or experimental applications such as determining cell size [13–15] and tissue temperature mapping [16, 17]. DWI is based on the effects of the microscopic brownian motion (diffusion) of water molecules in tissue. In addition to ϱ, T_1, or T_2 contrast, the strength of water diffusion directly influences signal intensity in diffusion-weighted images.

MRI sequences can be diffusion-sensitised by adding a pair of strong gradients, the Stejskal-Tanner method [18]. These gradients cause phase changes of the proton spins proportional to their stochastic spatial displacement and hence reduction in signal in the image depending directly on the local diffusion coefficient. The quantitative dependence between diffusion constant D and image intensity I is described by b, a parameter dependent on strength and timing (duration δ and separation of onset Δ) of the diffusion gradients (gyromagnetic ratio γ, gradient strength G) [18]:

$$\ln \frac{I(b)}{I_0} = -bD = -(\gamma G\delta)^2(\Delta - \frac{\delta}{3})\, D. \quad (1)$$

The apparent diffusion coefficient (ADC) can be calculated from two or more diffusion-weighted images with different b values; it is called "apparent" because it results from a mixture of intra- and extracellular diffusion coefficients and systematic shifts due to restricted diffusion effects [14, 19, 20]. The Stejskal-Tanner gradient scheme is widely used because it can be combined with different imaging techniques ranging from simple spin-echo (SE) to echo-planar imaging (EPI) [21–23].

An important limitation to the use of DWI in clinical practice is the frequent severe image degradation by involuntary patient motion. The two main components of motion in brain imaging are bulk movement (translation and rotation) of the head and periodic local movements of brain tissue due to cerebrospinal fluid pulsation. As a consequence of the sensitivity of DWI to stochastic motion in the micrometer range, the method is extremely susceptible to macroscopie motion of the object being imaged as well. Tissue motion in the submillimetre range during the diffusion-weighting period leads to severe image artefacts. Different approaches have been suggested for overcoming motion-induced artefacts [24], including multiple image averaging [25], radial projection

Table 1 Acquisition parameters of sequences (see also Fig. 1)

Sequence	SE	MSE 3	MSE 5
Number of spin-echo readouts	2	4	6
Number of image data readouts	1	3	5
Pseudo-echo time (T_{E1}) (ms)	100.0	90.0	90.0
Echo time for navigator T_{E2} (ms)	126.0	105.0	105.0
Inter-echo time T_{IE} (ms)	26.0	15.0	15.0
Image matrix (phase × readout)	159 × 192	162 × 192	160 × 200
Minimum field of view (mm)	80	100	100
Minimum slice thickness (mm)	1	5	5
Duration of diffusion gradients δ (ms)	37.5	36.9	36.9
Diffusion time Δ (ms)	45.4	45.0	45.0
Maximum b[a]	664	623	655
Acquisition time[a] (TR 1500 ms) (s)	245	98	65
Acquisition time[a] (pulse triggering) (s)	309	117	85

[a] The maximum b-values and the acquisition times refer to field of view 220 mm, acquisition of 4 slices, and TR 1500 ms (TR ≈ 1850 ms for pulse-triggered acquisition)

reconstruction [26], less bulk-motion sensitive sequences (e. g. using velocity-compensating gradients [27]), single-shot imaging methods such as high-speed STEAM [28], GRASE [29], or EPI [21–23], pulse triggering or cardiac gating [30], and the correction of data using navigator echoes. These are additional echoes acquired with constant phase-encoding, which differ from each other only in motion-induced phase shifts [31, 32]. These shifts can be calculated and applied inversely to the *k* space data to remove the effects of bulk motion and hence motion artefacts. Several studies have shown the benefit of navigator echo (NAV) correction of DWI [33–35].

Our objective was a quantitative evaluation of the efficacy of NAV correction and pulse triggering (cardiac gating) in DWI, separately or combined. Their efficacy was evaluated with three imaging sequences, taking into consideration acquisition time and image quality.

Methods

A conventional SE sequence and two sequences with multiple spin-echo (MSE) readout were implemented on a clinical 1.5-T image R with standard hardware (maximum gradient strength 15 mT/m, minimum rise time 750 μs). All sequences were extended with Stejskal-Tanner diffusion gradients and a navigator echo readout at constant (zero) phase encoding. The MSE sequences contained a series of 180° radio frequency pulses to acquire either three (MSE 3) or five (MSE 5) echoes after each excitation, which were used as image data. The total number of echoes acquired after each excitation, including the navigator echo, was thus 2 (SE), 4 or 6 (MSE). The sequence parameters are summarised in Table 1, and a diagram of the sequence scheme with navigator readout is shown in Fig. 1. The acquisition timing of all sequences could be synchronised with the pulse, using a photoplethysmograph finger pulse sensor.

An objective measure of the amount and severity of artefacts had to be established. The quotient of mean signal intensity outside and within the object being imaged was defined as the artefacticity *A* of the image, but because of the typical form of motion artefacts in DWI a slightly more complicated algorithm had to be used.

Determining the mean intensity I_0 within the object is difficult because motion artefacts result in image intensity spread all over the field of view (FOV) mainly in the phase-encoding direction. Hence, image intensity cannot be defined as the intensity in a certain region, and was redefined as the mean of the intensity of the brightest 30% of all image pixels, which, however, were not necessarily in the original area of the object. The empirically determined fraction of 30% of all pixels is sufficiently large to include a major portion of intense tissue, but it does not contain any background area. The corresponding intensity limit $I_{70\%}$ can be calculated from the integral $H(I)$ of the intensity histogram function $h(I)$ of the image:

$$H(I) = \int_0^I \mathrm{d}I'\, h(I'). \tag{2}$$

If $N = H(I_{max})$ is the total number of pixels, I_{max} the maximum pixel intensity, then, using the inverse function H^{-1}, the intensity limit to a given fraction f of all pixels is given by

$$I_f = H^{-1}(fN). \tag{3}$$

For example, $I_{70\%} = H^{-1}\ (0.7\ N)$ is the intensity limit such that 70% of all image pixels are less intense than $I_{70\%}$. The exact formula for the mean intensity of the object is:

$$I_0 = \int_{I_{70\%}}^{I_{98\%}} \mathrm{d}I'\, I'h(I') \Big/ \int_{I_{70\%}}^{I_{98\%}} \mathrm{d}I'h(I'). \tag{4}$$

The brightest 2% of all pixels were not taken into account to avoid bias by solitary intensity peaks due to reconstruction artefacts.

To determine the mean intensity I_M outside the original image area, which is caused by motion during acquisition, an elliptical mask was defined manually (Fig. 2). The mask was defined on a maximum-intensity projection of all slices of the images acquired without diffusion weighting ($b = 0$) and hence without severe motion artefacts. The intensity I_N of statistical noise was subtracted from I_M to determine motion-induced artefact intensity only. To calculate the noise intensity I_N, two horizontal background areas were defined in the oversampling region adjacent to the normal image (Fig. 2c); the regions above and below the object were not affected by motion artefacts. Image masks were defined separately for each individual. Artefacticity *A* was defined as:

$$A = \frac{I_M - I_N}{I_0}. \tag{5}$$

The same quantities were used to define the signal-to-noise ratio (SNR) of diffusion-weighted images:

$$R_{SN} = \frac{I_0}{I_N}. \tag{6}$$

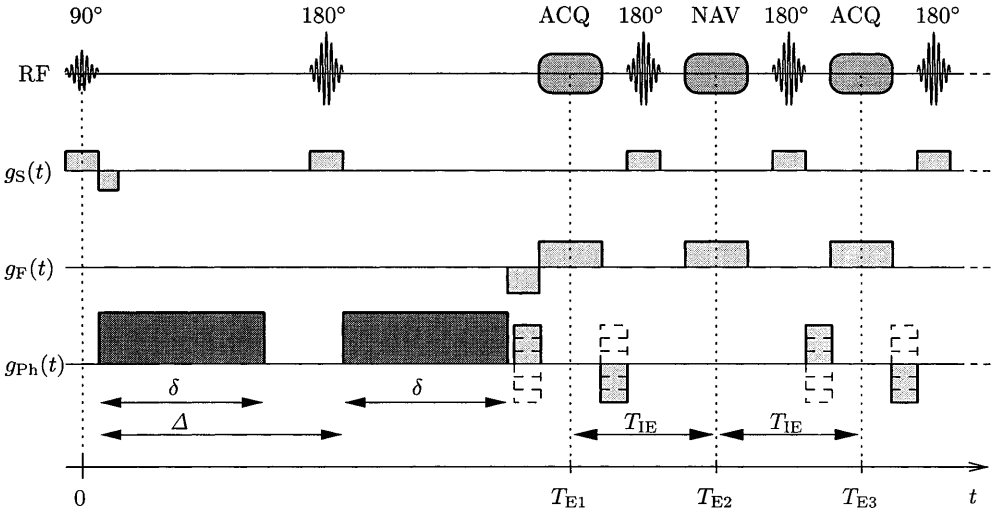

Fig. 1 MSE sequence scheme. The total number of acquisition echoes (ACQ) after each excitation is 3 or 5; the navigator echo (NAV) is inserted after the first ACQ. This scheme also applies to the SE sequence: in this case it ends after the NAV. See also Table 1

The results agree with the conventional definition of the SNR for average images. However, the particular form of the signal definition (I_0) leads to a SNR of about 1.7 for images containing only white noise; thus, a shift of SNR is to be expected in very noisy images.

We studied five healthy volunteers (4 men, 1 woman, age 25–31 years, mean 27 years). All sequences (SE, MSE 3, MSE 5) with navigator echo readout were used in all volunteers in three stages: 1. with diffusion gradients in the phase-encoding direction [34] and b 550 s mm^{-2}; repetition time (TR) 1500 ms; 2. with diffusion gradients in the phase-encoding direction and b 550 s mm^{-2}; acquisition synchronised with the pulse; TR was set at 2 cardiac cycles (about 1850 ms); and 3. without diffusion gradients ($b = 0$) and without pulse triggering; all other parameters as above (TR 1500 ms).

We acquired four axial images (thickness 5 mm, separation 15 mm) above the orbitomeatal line; the rectangular FOV was about 220 mm × 176 mm, varying slightly with matrix size (Table 1). Acquisition times ranged from 65 s to 309 s (Table 1). Since "ideal" co-operation could be expected from the volunteers (compared to a typical patient population), they were asked to minimise head motion during acquisition, but no head fixation or immobilisation was used.

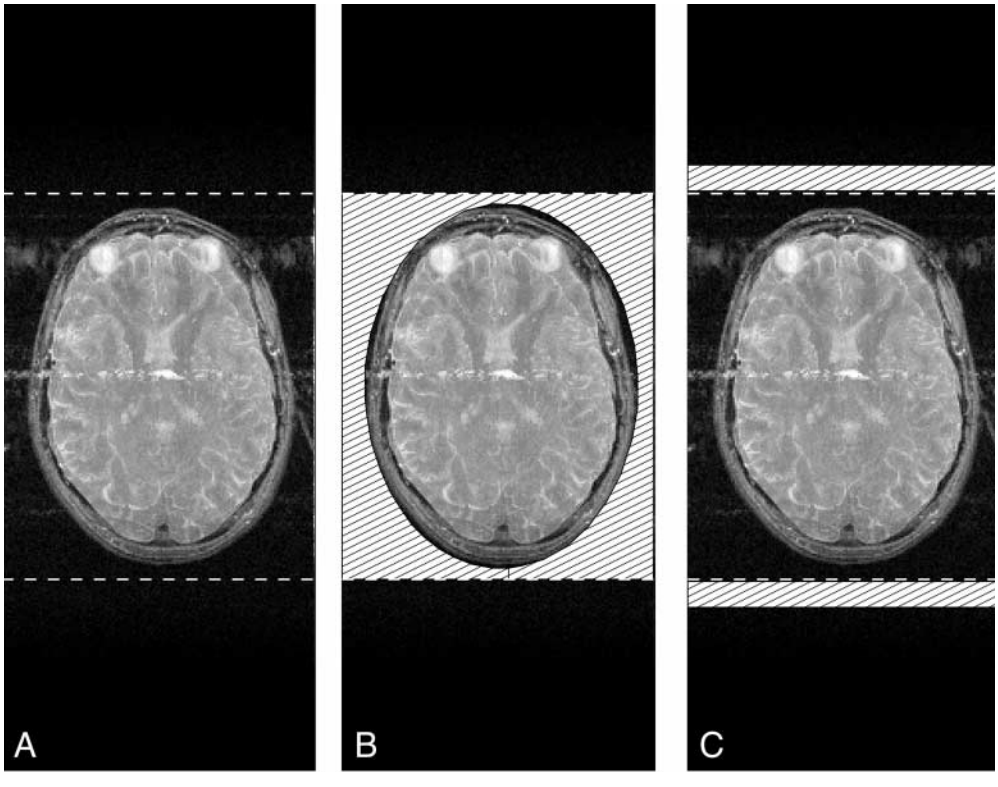

Fig. 2 A–C Image masks used for calculation of artefacticity. **A** Maximum-intensity projection through 4 slices acquired without diffusion weighting. The image is displayed with the oversampling area in the readout direction separated by dashed lines. **B** The *hatched region* was used to calculate the intensity I_M of motion artefacts. **C** Regions for calculation of background noise I_N

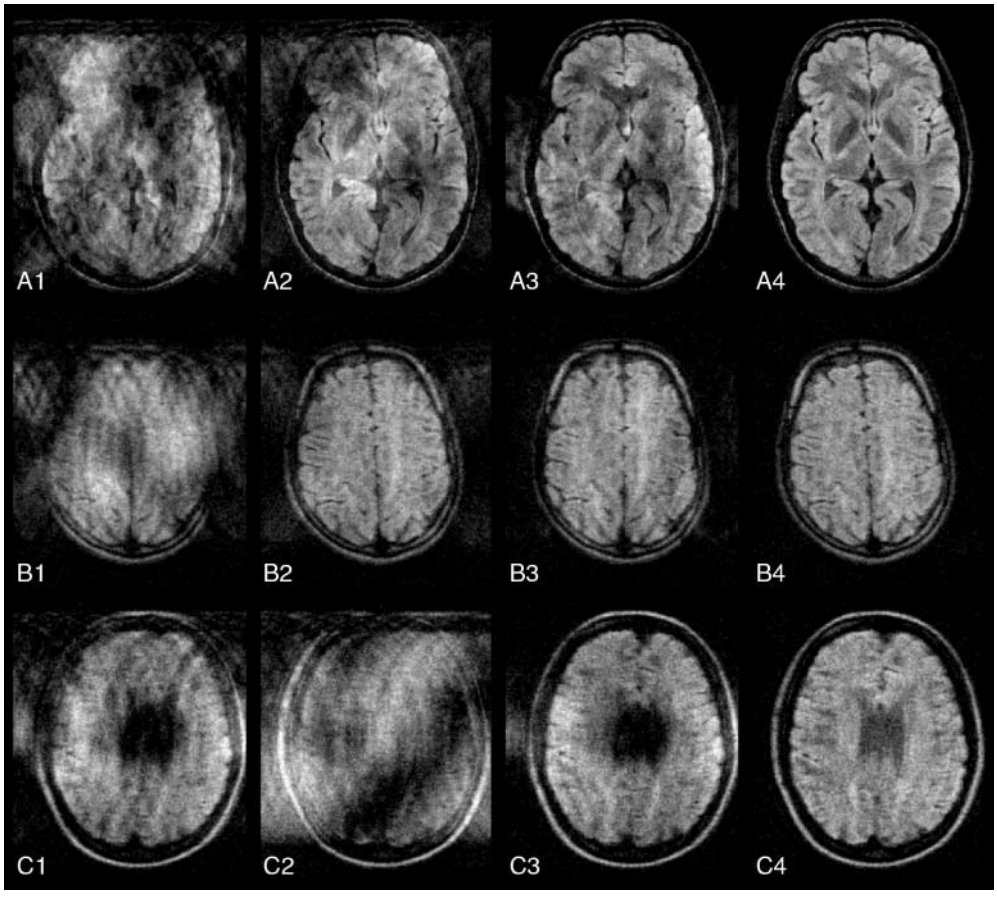

Fig. 3 A1–C4 Examples of advancing stages of motion correction for all sequences (**A** *SE;* **B** *MSE 3;* **C** *MSE 5*). *Column 1* uncorrected images, *2* acquisition with pulse triggering; *3* images after navigator echo-correction (NAV); *4* combination of pulse triggering and NAV correction. To present a broad variety of results, images in each row are from different volunteers and slice positions

After acquisition, the raw data were transferred to an external workstation, on which the NAV correction and data evaluation were performed using a self-written Matlab routine. From each acquisition two sets of images were reconstructed: one using and one discarding the additional motion information extracted from the NAV readout. These image sets were compared with each other and with the images from each of the three stages, to evaluate the efficacy of motion correction. The NAV correction we implemented did not use any fit algorithm to calculate head translation [33] or rotation [34] but applied the complete phase information extracted from the navigator echoes to the *k* space data. Mean values of artefacticity and SNR were calculated by averaging over all slices and all volunteers; this was carried out separately for original and corrected images from each acquisition pass and each sequence.

Results

Figure 3 demonstrates the efficacy of motion artefact reduction in DWI with pulse triggering and the NAV approach in examples from all three sequences. Image quality improves distinctly with advancing motion correction. Severe motion artefacts appear in the images without NAV correction on the left and right of the object, as a consequence of bulk head and pulsatile brain motion. The latter causes signal loss, particularly in the regions of the ventricles and on both sides of the ventricles in the vertical centre of the images. These vertically-centred artefacts remain after navigator correction alone, but are of much lower degree in slices located above the ventricles. The benefit of pulse triggering cannot be observed in image C2 because of presumably major head motion in this case. After combined application of pulse triggering and NAV correction, artefacts almost completely disappear. NAV correction worked successfully and without problems, independently of individual differences in type and degree of motion.

Comparison of the three fully motion-compensated sequences shows decreasing SNR and reduced image contrast from SE to MSE 5; however, the efficacy of motion artefact correction is similar. Calculated SNR values for pulse-triggered acquisitions are 12.3 ± 0.9 (SE), 8.5 ± 0.8 (MSE 3) and 8.1 ± 0.9 (MSE 5) (Fig. 4). Whereas a higher SNR is observed for acquisition without diffusion weighting, there is no significant difference if pulse triggering is used or not with diffusion-weighting.

The mean value of A is about 0.14 ± 0.05 for uncorrected data and 0.02 ± 0.01 for images after both pulse-triggered acquisition and NAV correction, con-

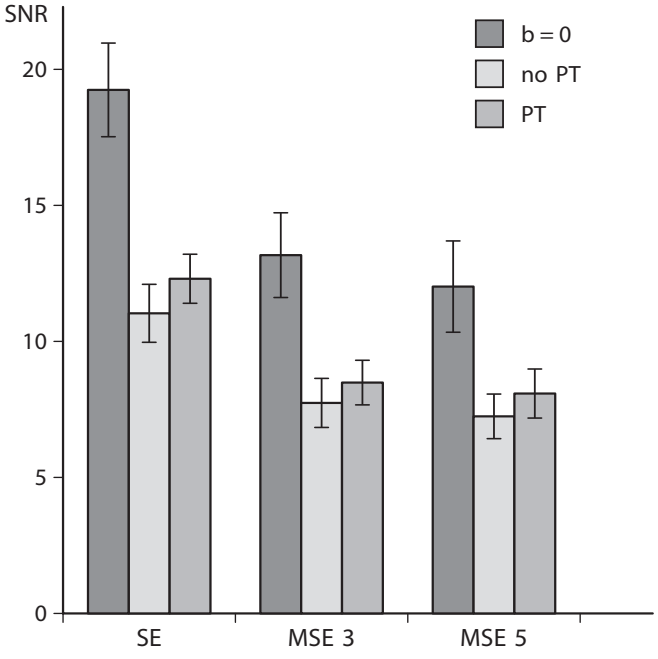

Fig. 4 Signal-to-noise ratio (SNR) for different sequences *(SE, MSE 3, MSE 5)* without diffusion weighting *(b = 0)*, with diffusion weighting but without pulse triggering *(no PT)*, and with both diffusion weighting and pulse triggering *(PT)*

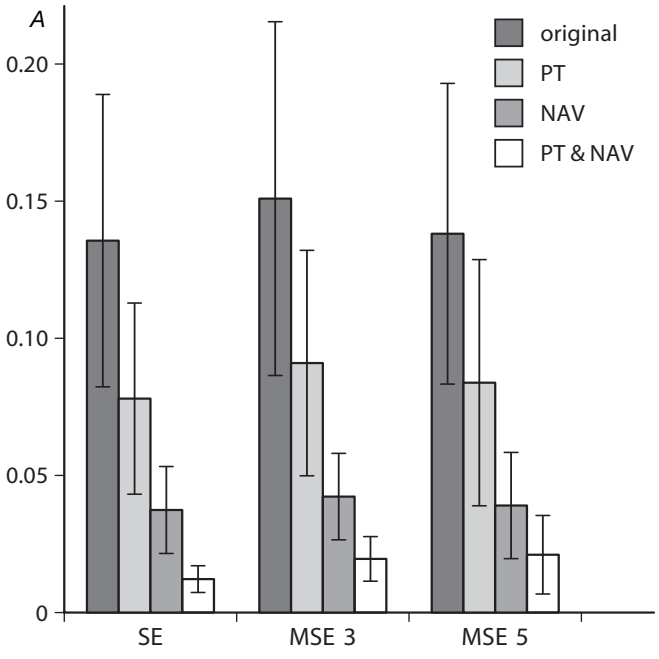

Fig. 5 Artifacticity *A* for different stages of motion correction (*PT* pulse triggering, *NAV* navigator correction) and three different sequences *(SE, MSE 3, MSE 5)*

sistently for all three sequences (Fig. 5). *A* is reduced by 91 % in SE, 87 % in MSE 3, and 84 % in MSE 5 images.

Discussion

Navigator echo correction combined with pulse-triggered acquisition provides a robust and efficient method for DWI on imagers with conventional gradient hardware. A significant reduction in motion artefacts is achieved, as reported for SE sequences with NAV correction [33–35]; in most cases no artefacts were visible after correction. The same is true for imaging with an extended readout of multiple echoes, which reduces acquisition time by a factor of 3–4.

Artefact reduction gains significantly more from NAV correction than from pulse triggering, which shows that bulk motion is generally more important than pulsatile brain motion. Above the ventricles, pulsatile brain motion seems negligible in many cases. However, this depends on the direction of the diffusion gradients, which was in-plane in our study and thus perpendicular to the main (radial) component of pulsatile motion above the ventricles. Acquiring with NAV correction alone can therefore be recommended for slices above the ventricles. The finger sensor can easily be applied, even after positioning the patient in the imager and thus may always be used to minimise the influence of pulsatile motion. The main disadvantage of pulse triggering is prolongation of acquisition time, depending on the rate and regularity of the pulse; in this volunteer study, acquisition time was extended by 20–30 %, but more prolongation should be expected in a typical patient population.

All three sequences gave similar results concerning motion sensitivity and correction. While the efficacy of motion correction was identical, image quality decreased with an increasing number of readout echoes and hence with decreasing acquisition time as a consequence of T_2 relaxation. This became evident as visibly reduced tissue contrast and decreasing SNR. Geometrical distortion or local image artefacts were not observed. For routine use, the quality of the fast MSE 5 images should prove adequate. However, if very high image quality is desired and acquisition time is not a limiting factor, the SE sequence with navigator correction and pulse triggering is recommended, because of its higher SNR. Sequences with more than five image echo readouts may be designed to speed acquisition, but lower SNR and inferior image quality must be expected. Without faster gradients, readout will be prolonged for such sequences, leading to stronger T_2 relaxation. The MSE 5 sequence appears to be a good compromise for the given gradient hardware.

Comparing these methods with diffusion-weighted single-shot EPI [23], the most frequently used alter-

native method for DWI, several arguments should be considered. The main advantages of single-shot EPI are insensitivity to bulk and pulsatile brain motion and the very short acquisition time. Image averaging can therefore be performed without unreasonably long acquisition times, and different diffusion gradients can be applied in one direction, to use more than two *b* values for ADC calculation, or in different directions to calculate diffusion tensor images [9]. On the other hand, EPI is typically affected by susceptibility [36] and eddy current [37] artefacts and depending on slice position, gross geometrical distortion; this is especially disadvantageous if superposition on morphologic images is desired. Another consequence of the relatively long EPI readout is inhomogeneous image contrast, due to T_2 and T_2* effects. Single-shot EPI requires extended gradient facilities with strong, fast-switching gradients, not available on many imagers. Therefore, if single-shot EPI cannot be performed because of hardware restrictions or if high image quality with minimal geometrical distortion is desired, the use of navigator-corrected, pulse-triggered MSE sequences is recommended.

To perform tensor imaging with a NAV-corrected sequence, it would be necessary to extend the sequence scheme. The sequences described can correct for rotational phase shifts only with the diffusion gradient in the phase direction [34]. For other diffusion directions, the navigator echo should be acquired not only in the readout direction but as 2D (e. g. spiral) navigator, requiring a much more complicated correction algorithm; otherwise, only the translational component of bulk motion can be corrected. Because of the long acquisition time for tensor imaging without single-shot sequences, this approach was not investigated further.

Multiple signal averaging as another method to suppress motion artefacts requires a much longer acquisition time, depending on the number of averages (usually 4–16 [25]), whereas the navigator readout can be added without significant prolongation of acquisition. While the use of flow-compensated gradients has the disadvantage (similar to most single-shot methods) that an advanced gradient system is needed, the NAV correction requires only standard imaging gradients.

References

1. Moseley ME, Cohen Y, Mintorovitch J, Chileuitt L, Shimizu H, Kucharczyk J, Wendland MF, Weinstein PR (1990) Early detection of regional cerebral ischemia in cats: comparison of diffusion- and T2-weighted MRI and spectroscopy. Magn Reson Med 14: 330–346
2. Moseley ME, Kucharczyk J, Mintorovitch J, Cohen Y, Kurhanewicz J, Derugin N, Asgari H, Norman D (1990) Diffusion-weighted MR imaging of acute stroke: correlation with T2-weighted and magnetic susceptibility-enhanced MR imaging in cats. AJNR 11: 423–429
3. Lövblad KO, Baird AE, Schlaug G, Benfield A, Siewert B, Voetsch B, Connor A, Burzynski C, Edelman RR, Warach S (1997) Ischemic lesion volumes in acute stroke by diffusion-weighted magnetic resonance imaging correlate with clinical outcome. Ann Neurol 42: 164–170
4. Tong DC, Yenari MA, Albers GW, O'Brien M, Marks MP, Moseley ME (1998) Correlation of perfusion- and diffusion-weighted MRI with NIHSS score in acute (< 6.5 hour) ischemic stroke. Neurology 50: 864–870
5. Singer MB, Chong J, Lu D, Schonewille WJ, Tuhrim S, Atlas SW (1998) Diffusion-weighted MRI in acute subcortical infarction. Stroke 29: 133–136
6. Fischer M, Bockhorst K, Hoehn-Berlage M, Schmitz B, Hossmann KA (1995) Imaging of the apparent diffusion coefficient for the evaluation of cerebral metabolic recovery after cardiac arrest. Magn Reson Imaging 13: 781–790
7. Tarr RW (1997) Brain attack. Clinical monitoring of early pathophysiologic events. Neurosurg Clin North Am 8: 179–194
8. Hossmann KA, Hoehn-Berlage M (1995) Diffusion and perfusion MR imaging of cerebral ischemia. Cerebrovasc Brain Metab Rev 7: 187–217
9. Douek P, Turner R, Pekar J, Patronas N, Le Bihan D (1991) MR color mapping of myelin fiber orientation. J Comput Assist Tomogr 15: 923–929
10. Brunberg JA, Chenevert TL, McKeever PE, Ross DA, Junck LR, Muraszko KM, Dauser R, Pipe JG, Betley AT (1995) In vivo MR determination of water diffusion coefficients and diffusion anisotropy: correlation with structural alteration in gliomas of the cerebral hemispheres. AJNR 16: 361–371
11. Pierpaoli C, Jezzard P, Basser PJ, Barnett A, Di Chiro G (1996) Diffusion tensor MR imaging of the human brain. Radiology 201: 637–648
12. Buchsbaum MS, Tang CY, Peled S, Gudbjartsson H, Lu D, Hazlett EA, Downhill J, Haznedar M, Fallon JH, Atlas SW (1998) MRI white matter diffusion anisotropy and PET metabolic rate in schizophrenia. Neuroreport 9: 425–430
13. Anderson AW, Zhong J, Petroff OA, Szafer A, Ransom BR, Prichard JW, Gore JC (1996) Effects of osmotically driven cell volume changes on diffusion-weighted imaging of the rat optic nerve. Magn Reson Med 35: 162–167
14. Pilatus U, Shim H, Artemov D, Davis D, van Zijl PC, Glickson JD (1997) Intracellular volume and apparent diffusion constants of perfused cancer cell cultures, as measured by NMR. Magn Reson Med 37: 825–832
15. Kuchel PW, Coy A, Stilbs P (1997) NMR "diffusion-diffraction" of water revealing alignment of erythrocytes in a magnetic field and their dimensions and membrane transport characteristics. Magn Reson Med 37: 637–643
16. Bleier AR, Jolesz FA, Cohen MS, Weisskoff RM, Dalcanton JJ, Higuchi N, Feinberg DA, Rosen BR, McKinstry RC, Hushek SG (1991) Real-time magnetic resonance imaging of laser heat deposition in tissue. Magn Reson Med 21: 132–137

17. MacFall J, Prescott DM, Fullar E, Samulski TV (1995) Temperature dependence of canine brain tissue diffusion coefficient measured in vivo with magnetic resonance echo-planar imaging. Int J Hyperthermia 11: 73–86
18. Stejskal OE, Tanner JE (1965) Spin diffusion measurements: spin echoes in the presence of a time-dependent field gradient. J Chem Phys 42: 288–292
19. Norris DG, Niendorf T, Hoehn-Berlage M, Kohno K, Schneider EJ, Hainz P, Hropot M, Leibfritz D (1994) Incidence of apparent restricted diffusion in three different models of cerebral infarction. Magn Reson Imaging 12: 1175–1182
20. Stanisz GJ, Szafer A, Wright GA, Henkelman RM (1997) An analytical model of restricted diffusion in bovine optic nerve. Magn Reson Med 37: 103–111
21. Turner R, Le Bihan D, Maier J, Vavrek R, Hedges LK, Pekar J (1990) Echo-planar imaging of intravoxel incoherent motion. Radiology 177: 407–414
22. Stehling MK, Turner R, Mansfield P (1991) Echo-planar imaging: magnetic resonance imaging in a fraction of a second. Science 254: 43–50
23. Turner R, Le Bihan D, Chesnick AS (1991) Echo-planar imaging of diffusion and perfusion. Magn Reson Med 19: 247–253
24. Trouard TP, Sabharwal Y, Altbach MI, Gmitro AF (1996) Analysis and comparison of motion-correction techniques in diffusion-weighted imaging. J Magn Reson Imaging 6: 925–935
25. Merboldt KD, Hänicke W, Gyngell ML, Frahm J, Bruhn H (1989) The influence of flow and motion in MRI of diffusion using a modified CE-FAST sequence. Magn Reson Med 12: 198–208
26. Gmitro AF, Alexander AL (1993) Use of a projection reconstruction method to decrease motion sensitivity in diffusion-weighted MRI. Magn Reson Med 29: 835–838
27. Brockstedt S, Thomsen C, Wirestam R, De Poorter J, De Wagter C, Salford LG, Holtås S, Stahlberg F (1995) Use of an enhanced gradient system for diffusion MR imaging with motion-artifact reduction. Acta Radiol 36: 662–670
28. Merboldt KD, Hänicke W, Bruhn H, Gyngell ML, Frahm J (1992) Diffusion imaging of the human brain in vivo using high-speed STEAM MRI. Magn Reson Med 23: 179–192
29. Johnson G, Feinberg DA, Venkataraman V (1996) Single-shot GRASE imaging with short effective TEs. J Magn Reson Imaging 6: 944–947
30. Posse S, Cuenod CA, Le Bihan D (1993) Human brain: proton diffusion MR spectroscopy. Radiology 188: 719–725
31. Ehman RL, Felmlee JP (1989) Adaptive technique for high-definition MR imaging of moving structures. Radiology 173: 255–263
32. Korin HW, Felmlee JP, Ehman RL, Riederer SJ (1990) Adaptive technique for three-dimensional MR imaging of moving structures. Radiology 177: 217–221
33. Ordidge RJ, Helpern JA, Qing ZX, Knight RA, Nagesh V (1994) Correction of motional artifacts in diffusion-weighted MR images using navigator echoes. Magn Reson Imaging 12: 455–460
34. Anderson AW, Gore JC (1994) Analysis and correction of motion artifacts in diffusion weighted imaging. Magn Reson Med 32: 379–387
35. de Crespigny AJ, Marks MP, Enzmann DR, Moseley ME (1995) Navigated diffusion imaging of normal and ischemic human brain. Magn Reson Med 33: 720–728
36. Lövblad KO, Jakob PM, Chen Q, Baird AE, Schlaug G, Warach S, Edelman RR (1998) Turbo spin-echo diffusion-weighted MR of ischemic stroke. AJNR 19: 201–208
37. Alexander AL, Tsuruda JS, Parker DL (1997) Elimination of eddy current artifacts in diffusion-weighted echo-planar images: the use of bipolar gradients. Magn Reson Med 38: 1016–1021